Aerodynamic Load Control through Blowing

N. Al-Battal[1], D. J. Cleaver[2] and I. Gursul[3]
Department of Mechanical Engineering, University of Bath, Bath, BA2 7AY, UK

Aircraft are subject to extreme loads during gust encounters. Amelioration of these loads will allow for reduced structural weight and therefore greater efficiency. In this paper, two versions of blowing jet from suction surface, normal and upstream, are studied under steady state conditions to illustrate the effectiveness of these devices at mitigating extreme lift. Force, pressure and Particle Image Velocimetry measurements were performed at a Reynolds number of 660,000 for a NACA 0012 airfoil. A range of volumetric flow rate coefficients, below C_Q = 0.44%, for a range of angles of attack 0° ≤ α ≤ 20°, are studied for five chordwise locations. It was observed that normal blowing at x_J/c = 0.95 induces a change in lift of ΔC_L = -0.15 for the maximum momentum coefficient. Locations further forward produce a negligible change in lift coefficient. Whereas, upstream blowing was capable of reducing lift at all chordwise locations studied by up to ΔC_L = -0.33. Upstream blowing encourages the shear layer to deflect upwards and inciting a greater adverse pressure gradient on the upper surface. Locations near the trailing edge are preferable for low angles of attack, as greater lift mitigation is obtained. Lift reduction can be augmented for higher angles of attack, with leading edge locations. As expected, increasing momentum coefficient increases the magnitude of the change in lift for all cases studied.

Nomenclature

C_L	=	lift coefficient	α	=	angle of attack
C_p	=	pressure coefficient	ρ_J	=	density of jet air
C_Q	=	volumetric flow rate coefficient	ρ_∞	=	density of freestream flow
C_μ	=	momentum coefficient	x_J	=	location of jet
c	=	chord	U_J	=	jet velocity
ΔC_L	=	change in lift coefficient relative to baseline	U_∞	=	freestream velocity
h_J	=	slot width			
Re	=	Reynolds number			
s	=	span			

I. Introduction

GUSTS are often the critical load cases for the design of aircraft and therefore dictate the mass of the structure. In addition they are detrimental to passenger comfort. Gust encounters therefore significantly impact the efficiency and performance of the aircraft. Current gust load alleviation techniques comprise of ailerons and spoilers, which exhibit low frequency response (≈ 6 Hz), relative to the gust frequency (≈ 15 Hz), due to their large inertia. Therefore, it becomes a salient issue to realize an alternative method which can effectively ameliorate gust loads with fast frequency response. Unsteady fluidic actuators, such as synthetic jets and oscillating jets, have shown to prevent flow separation and augment lift successfully at high frequencies[1-4]. However, such actuators are yet to be investigated experimentally to determine their capability for reducing lift. The jet, or jet flap, is proposed as one possible high frequency alternative to current technologies.

[1] Postgraduate Student, Department of Mechanical Engineering, Student Member AIAA.
[2] Lecturer, Department of Mechanical Engineering, Member AIAA.
[3] Professor, Department of Mechanical Engineering, Associate Fellow AIAA .

The jet, often placed at the trailing edge of the lower surface, acts by utilizing high momentum flow ejected normal to the surface to deflect cross-flow streamlines[5]. When blown downstream, the jet can prevent flow from separating from the surface of the wing. This engenders circulation which increases beyond the 'natural state'. CFD investigations showed that a downstream blown jet with a jet velocity ratio of 2, located at mid-chord of a NACA 0015 airfoil, creates a change in lift of ΔC_L = 0.17 at the point of stall[6]. The strength of the jet is generally characterized by the momentum coefficient, C_μ[7]:

$$C_\mu = \frac{\rho_J h_J U_J^2}{\frac{1}{2}\rho_\infty U_\infty^2 c} \tag{1}$$

Spence[9] performed theoretical calculations, to postulate that the change in lift due to the jet is directly proportional to the root of momentum coefficient. This statement has been corroborated in studies[5,10,11] with jet deflection angles less than 70°, and it has also been shown that a jet deflection of 90° will invalidate the theory, regardless of momentum coefficient value, due to flow separation. However, Traub et *al.*[12] showed for values up to C_μ = 3.0%, a jet ejected normal to the lower surface upholds the relationship. When considering jets for alleviating lift, Boeije et *al.*[8] performed computational studies for a NACA 0018 at α = 0°, which indicate a change in lift coefficient ΔC_l = -0.5 could be achieved when a normal jet, of C_μ = 1.75%, is placed on the upper surface, at x_J/c = 0.90. However, this change in lift diminishes at greater angles due to the jet being immersed within the boundary layer. To the authors' knowledge, experimental studies are yet to be performed for jets on the upper surface.

In this paper, the jet will be investigated in two different configurations; ejected normal to the upper surface, and upstream, opposing the free-stream velocity, see Fig. 1. The two configurations will be assessed and compared for their capabilities at reducing lift under steady state conditions. This study will be extended to unsteady jets as a next step.

II. Experimental Techniques

Experiments were performed in a low-speed closed-circuit wind tunnel at the University of Bath. The wind tunnel has a working test section length of 2770 mm, with a height and width of 1510 mm and 2120 mm, respectively. Hot wire measurements show the turbulence intensity of the wind tunnel is below 0.5%. The free-stream velocity was set to 20 ms^{-1}, which equates to a Reynolds number of *Re* = 660,000. To induce a fixed transition point, a trip wire has previously been shown to be effective for NACA four-digit wings[13,14]. Experiments with many different trip devices suggested that a trip wire of 0.3 mm at x/c = 0.10 on the upper and lower surface is a good choice.

A. Experimental Setup

The symmetrical NACA0012 airfoil, was chosen for experiments. The airfoil has a 500 mm chord length and 1500 mm span. It spanned the test section, wall to wall, so as to create an infinite wing. The wing was manufactured in two separate parts. The first 75% of the chord length was made from a carbon fibre composite, and stiffened with the combination of Rohacell® XT foam and an internal aluminium alloy framework. Due to the intricate internal design, the remaining 25% of the chord length was rapid prototyped using DuraForm® PA plastic. Porous polyethylene sheets of 2 mm thickeness were closely situated underneath the jet exit, to ensure flow emanated from the jet uniformly across the entire span. Hot wire measurements carried out at each chordwise jet location, along 59 equally spaced spanwise locations, confirmed that the jet velocity at any point deviated less than 10% from the mean velocity. The jet slot was designed to have a width of 1 mm, and span the entire wing, in order to maintain quasi two-dimensional flow conditions. Aluminium tubes located within the wing at x_J/c = 0.08 & 0.60, act as plenum chambers. The remaining jet locations are situated in the rapid prototyped section, which utilizes the entire internal space as the plenum chamber. Jet slots were constructed to discharge air normal to the surface of the wing. Upstream blowing was achieved by adding an additional carbon fibre piece on to the surface of the wing, as shown in Fig. 2a. The piece provides a protruded step of 0.5 mm (0.1% c), and extends 5 mm (1% c) ahead of the jet slot. Force measurements for zero jet velocity confirmed the addition of the piece had negligible effect on the force generated across all angles of attack. The volumetric flow rate coefficient for a two-dimensional jet can be defined as:

$$C_Q = \frac{h_J U_j}{U_\infty c} \tag{2}$$

Five locations for the jet were selected at x_j/c = 0.08, 0.60, 0.75, 0.85 & 0.95. The strength of the jet is defined using a non-dimensional parameter, coefficient of momentum, C_μ. The jet momentum coefficients utilized for this investigation are C_μ = 0.8%, 1.6%, 2.4%, 3.2% & 4.0% for upstream blowing. As the slot width for normal blowing is twice that of upstream blowing, the jet velocity is halved; the corresponding momentum coefficients used for normal blowing are C_μ = 0.4%, 0.8%, 1.2%, 1.6% & 2.0%. As such, the volumetric flow rate coefficient (C_Q = 0.44%) is maintained between C_μ = 2.0% for normal blowing and C_μ = 4.0% for upstream blowing to preserve the same work rate. A calibration curve to relate the mass flow rate to the momentum coefficient was obtained for a volumetric flow rate range of 0 to 3000 LPM, at 20 distinct interval points. The regulated air supply for the jets was sourced from Departmental compressors with a pressure of 7 bar. The volumetric flow rates for the jet were determined using a SMC® PF2A703H-10-68 digital flow switch, which has an uncertainty of ±1%.

B. Force Measurements

A two component binocular strain gauge force balance was manufactured from 2014 T6 Aluminium alloy. The wing was mounted below the force balance as a cantilever. The strain gauges were excited using a Wheatstone bridge configuration, with an excitation voltage of 5 V. Voltage signals were converted and amplified using a 12-bit analogue to digital converter. A Force-to-Voltage calibration was obtained by applying known weights to the wing. These calibration curves consisted of 16 data points, ranging from 0 to 150 N. Lift and drag forces were recorded using LABVIEW® 7.1, at a sample rate of 2 kHz for 20,000 samples, which was repeated three times and averaged to ensure accuracy of the measurements. Processing was carried out using MATLAB® to determine the force values recorded for a range of angles of attack between $0° \leq \alpha \leq 20°$.

C. Pressure Measurements

Pressure measurements were taken from 40 pressure taps, which were situated at the mid-span. The pressure taps setup comprised of 19 pressure taps on the upper surface, and 21 taps on the lower surface. Presence of the upper surface jet slots made it difficult to have an equal number of pressure taps on both surfaces. A Scanivalve Corp PDCR23 differential pressure transducer was utilized to measure pressure. Calibration of the differential pressure transducer was taken with the use of a Druck DPI portable transducer calibrator. A sample frequency of 1 kHz was used and three repeats of each case was taken to produce time-averaged pressure measurements.

D. Particle Image Velocimetry

The velocity field was measured for the upper surface of the airfoil. A six-jet TSI® oil droplet generator 9037-6 was used to seed the wind tunnel, with atomized olive oil droplets with an average size of 1 µm. The droplets were illuminated using the EverGreen 200 mJ 15Hz Nd:YAG double-pulse dual laser. The laser was positioned perpendicular to the wing, forming an obscured view of the lower surface, see Fig. 2b. As shown in Fig. 2b, two TSI® PowerView™ CCD 8MP cameras were placed 1200 mm below the laser plane, with two Nikon AF 50 mm NIKKOR f/1.8D lenses. Two cameras were required to cover the entire region of interest with a good degree of accuracy and had an overlap region of 35 mm. The TSI® LaserPulse 610034 synchroniser was used to synchronise laser pulses with the image captures. The images are analysed and generated using a recursive FFT cross-correlator within the TSI® Insight 3G software. An interrogation window size of 32 x 32 pixels provided a spatial resolution of 4 mm.

Velocity field data was derived from a time-average of 450 image pairs. Further processing using MATLAB® merged the data from the two cameras to produce a single data set. Data was collected for C_μ = 0.8%, 2.4% & 4.0%, at chordwise locations of x_j/c = 0.08, 0.60 & 0.95, for angles of attack at α = 0°, 5°, 8°, 10°, 13° and 16°. However, only the results for C_μ = 4.0% for α = 0°, 5°, 8° & 13° at all three chordwise locations are presented here.

E. Uncertainty Analysis

Uncertainty errors are determined using methods posited by Moffat[15]. Uncertainty of dynamic pressure readings from within the wind tunnel were determined to be 1.6%. Lift coefficient uncertainties were determined to be 2.1%. Momentum coefficient uncertainty comprised of errors contributing from variables such as hot wire measurements and area of jet slot. Consequently, uncertainty for momentum coefficient was determined to be 2.6%. In addition, angle of attack had an uncertainty of 0.25°.

III. Results and Discussion

A. Effect of Blowing Direction

For comparison shown in Fig. 3 is the baseline case which represents the unforced case. Experimental studies for NACA 0012 airfoils, at similar Reynolds numbers[16-18], of the order 10^5, closely agree with these results. Shown in Fig. 3, is time-averaged lift coefficients for upstream blowing and normal blowing, at three chordwise locations with a maximum volumetric flow rate of C_Q = 0.44%. The maximum volumetric flow rate corresponds to momentum coefficients of C_μ = 2.0% and C_μ = 4.0% for normal blowing and upstream blowing, respectively. Normal blowing at x_J/c = 0.08, begins to increase lift coefficient at α = 5°, relative to the baseline, up until the point of stall. An average increase in lift coefficient of ΔC_L = 0.06 is realized for angles between 5°- 11°. Hence, normal blowing does not induce a lift reduction when placed near the leading edge. When the normal jet is located at x_J/c = 0.60, no change in lift is observed. It is only when the normal jet is positioned closer to the trailing edge that a significant loss in lift is attained. When employed at x_J/c = 0.95, a momentum coefficient of C_μ = 2.0% gives a consistent change in lift of ΔC_L ≈ -0.15. Such a change would be sufficient for aircraft in cruise.

Further reduction in lift can be achieved when employing upstream blowing at all chordwise locations. For x_J/c = 0.08, the effectiveness of lift reduction is dependent on the angle of attack, so that larger angles create greater change in lift. In addition, stall angle is delayed to 19°. Similar behavior is observed for x_J/c = 0.60, although effect is diminished. Upstream blowing at x_J/c = 0.95 creates the same behavior as normal blowing but amplified by approximately 33%. As such, the enhanced lift mitigation for upstream blowing means that it will be the focus of future measurements. It is important to note the momentum coefficient differs in this comparison but the flow coefficient C_Q, which represents work and is therefore more practically relevant, remains the same.

A comparison can be made by past experiments for jet flaps employed near the trailing-edge. Spence postulated a square-root relationship with the change in lift[9], for trailing edge jets, shown in eq. (3). As such, Fig. 4a compares the data collected at the University of Bath, for upstream and normal blowing jets, at all chordwise locations for the range of momentum coefficient values considered, with experimental data from literature at α = 0°. Experimental data presented are representative of jets on the lower surface[5,12,20-21], for the purpose of increasing lift. The theoretical line plotted is fitted using literature data alone. From the figure, it is deduced that the data collected confirm Spence's theory can be applied for jets on the upper surface. Data collected by Traub et *al.*[12] were the most analogous to the normal blowing jet. For this angle of attack at x_J/c = 0.95, normal and upstream blowing approximately collapses onto a single curve. This suggests momentum coefficient is a suitable parameter for this angle. A loss in effectiveness occurs with jets closer to the leading edge. This becomes more pronounced with normal blowing; no change in lift for normal blowing at x_J/c = 0.75, as opposed to small lift change for x_J/c = 0.08 with upstream blowing.

$$\Delta C_L \propto \sqrt{C_\mu} \tag{3}$$

Figure 4b compares data collected at α = 13° for upstream and normal blowing jets. Upstream blowing is always preferable for reducing lift, regardless of location. The figure indicates that using momentum coefficient to compare the two blowing directional methods is not appropriate for this angle. One would expect data for common momentum coefficients, between the two methods, to superimpose with one another on the curve. However, the general lack of agreement between the two methods is observed for lower angles of attack. As such, coefficient of volumetric flow rate is considered to be a fairer parameter of measurement when comparing blowing directions because it represents the work done.

Figure 5, shows the time-averaged velocity fields comparing normal blowing and upstream blowing with the baseline case, for x_J/c = 0.95; this equates to Fig. 3c. For the α = 0° cases when PIV images are analyzed with smaller grid size, the normal jet induces a separation point immediately at the location of the jet, thereby creating a separated region encompassing the region between the jet and the trailing edge. Two counter-rotating vortices can be seen inside the recirculation zone. The separated region causes flow outside the region to be deflected upwards. The normal jet has a significant influence on flow from the lower surface, as it is entrained towards the upper surface. Such entrainment enhances the upwash effect within the wake of the airfoil. The ability of the normal jet to entrain flow from the lower surface is enhanced when placed near the trailing edge. Such closeness allows the normal jet to manipulate the Kutta condition of the airfoil, and therefore, the circulation. The flow field behavior resembles the CFD findings of Blaylock et *al*[19], for a jet flap employed at x_J/c = 0.95 on the lower surface. The slight camber effect on the upper surface causes a change in lift of ΔC_L = -0.15.

For upstream blowing the point of separation has moved upstream outside of the range of view in the close-up, thereby influencing a greater region of the airfoil in comparison to normal blowing. A greater separation region will not only affect the pressure gradient along the airfoil, but also increase the camber towards the trailing edge. This will inevitably produce a greater change in lift, in agreement with the force measurements discussed earlier. The behavior observed agrees with the force measurements considered in the last section. The increased separated region, caused by the upstream jet, causes a greater reduction in lift.

For the α = 5° baseline case, the leading edge region on the upper surface experiences an augmentation in local velocity magnitude. However, this region of high velocity magnitude is seen to diminish when deploying the normal blowing jet, as well as the upstream blowing jet. The normal blowing jet continues to deflect local flow upwards to retain the effective camber change, as exhibited in the α = 0° case. However, with upstream blowing, deflection of the streamlines initiates ahead of the jet location. In addition, a visible reduction in local velocity magnitude becomes apparent at this angle.

Similar behavior is demonstrated for normal blowing at α = 8°. The influence of upstream blowing propagates upstream with angle of attack to create an observable separated region. This difference in behavior agrees with the force measurements presented in Fig. 3c; normal blowing produces a change in lift of ΔC_L = -0.11, as upstream blowing produces a change in lift of ΔC_L = -0.17.

Testing at α = 13°, the baseline airfoil case exhibits a large separated region along the upper surface. When initiating the normal blowing jet, momentum is injected into the local region, thereby accelerating flow to induce a change in lift of ΔC_L = -0.08. Furthermore, the close up image of the normal blowing jet, confirms that the local flow continues to be deflected upwards, which is consistent with the behavior observed at earlier angles of attack. Upstream blowing injects momentum which impinges with the freestream velocity enlarging the separated region to create a recirculation zone. This behavior induces a change in lift of ΔC_L = -0.20, therefore confirming that upstream blowing maintains a relatively constant change in lift in comparison to normal blowing.

B. Force Measurements for Upstream Blowing

Presented in Fig. 6 are time-averaged force measurements for upstream blowing, at all chordwise locations and all momentum coefficient values. The left column is lift coefficient; the right column is change in lift coefficient relative to the baseline. When placing the upstream jet at x_J/c = 0.08, at higher angles of attack even the smallest momentum coefficient is sufficient enough to evoke a lift reduction. Furthermore, when utilizing a momentum coefficient of C_μ = 0.8%, the stall angle is brought earlier to α = 11°, from the baseline case of α = 13°. As the momentum coefficient increases, the gradient of the lift curve gradually decreases and the point of stall angle becomes less discernible. The effect of C_μ is most evident at α = 10°, beyond which, the curves converge to α = 13° where negligible difference is observed between each momentum coefficient. At α = 13°, the change in lift is approximately $\Delta C_L \approx 0.30$, which indicates that the upstream jet at x_J/c = 0.08, is suited to larger angles of attack. At low angles upstream blowing at α = 5° can reduce lift by ΔC_L = -0.03 for C_μ = 0.8%, ΔC_L = -0.07 with C_μ = 4.0%.

In Fig. 6b, time-averaged force measurements for upstream blowing at x_J/c = 0.60 show that change in lift is small until $\alpha \geq 9°$, when using a momentum coefficient of C_μ = 0.8%. A distinct relationship between change in lift and momentum coefficient appears, indicating that there is significant benefit to increasing the momentum coefficient for this location. Consequently, a reduction in lift of ΔC_L = -0.09 was acquired at α = 5° for C_μ = 4.0%. This shows that the jet at x_J/c = 0.60 performs better at lower angles of attack, in comparison to the upstream jet at x_J/c = 0.08. However, the change between each lift curve appears to reduce with increasing momentum coefficient, which implies an asymptote.

Figure 6c shows the time-averaged force measurements for the upstream jet configuration at x_J/c = 0.95. For this location all momentum coefficients produce an approximately linear trend towards a common stall angle of α = 14°. It is apparent that the performance of upstream blowing at x_J/c = 0.95, for low angles of attack is greatly improved; as C_μ = 0.8% at α = 5° reduces lift by ΔC_L = -0.11, exceeding the lift reduction achieved by jets at chordwise locations x_J/c = 0.08 and x_J/c = 0.60, for C_μ = 4.0%. A momentum coefficient of C_μ = 4.0% at the same angle of attack, amplifies this reduction to ΔC_L = -0.18. The effect of increasing momentum coefficient is to increase the gradient of the lift curve so that it becomes more effective at low angles of attack.

C. Effect of Varying Upstream Blowing Location

Shown in Fig. 7 is a force measurement comparison of chordwise locations for C_μ = 4.0%. As noted earlier, trailing-edge locations are preferable at low angles of attack. This is confirmed in Fig. 7, as the jet progressively moves from near the leading edge towards the trailing edge, lift reduction increases at low angles of attack but decreases at high

angles of attack. As a result a point of intersection is observed between α = 9° and 11°. At α = 2°, the baseline case induced a lift coefficient of C_L = 0.17; however, the jet produced a change in lift coefficient of ΔC_L = -0.11, -0.16 & -0.20 for the jet at x_J/c = 0.75, 0.85 & 0.95, respectively. Furthermore, upstream blowing, at all chordwise locations, extends its influence to beyond the stall angle to maintain the lift reduction. This implies that upstream blowing has a significant effect on the separated region on the upper surface; this is confirmed by the PIV measurements.

Time-averaged velocity fields for baseline and upstream blowing, at three chordwise locations are presented in Fig. 8. Upstream blowing appears to induce different behavior when varying the chordwise position. At x_J/c = 0.08, the velocity magnitude immediately downstream of the jet is seen to accelerate at α = 0°, confirmed in Fig. 9a by the increase in suction when compared to the baseline case. However, lift coefficient measurements (Fig. 7) indicates that this change in velocity magnitude is inadequate to produce a change in lift. Fig. 9a shows that pressure behind the jet location, is increased along the upper surface, but is also increased on the lower surface. In comparison, the jet at x_J/c = 0.60 decelerates the flow ahead of jet, before augmenting above the jet. Within this region, the pressure measurements suggest an increase in pressure is attained. Flow emanating from the jet impinges with the oncoming freestream flow. The effect is transposed ahead of the jet, where suction is lost. Downstream of the jet, the airfoil is subjected to greater suction, therefore mitigating any lift losses, as this equates to a change in lift coefficient of ΔC_L = -0.05. With the jet at x_J/c = 0.95, an increase in camber towards the trailing edge is created which engenders an upwash effect, in conjunction with flow entrainment from the lower surface. In addition, pressure along the entire upper surface is increased (see Fig. 9a) which ultimately causes reduction in lift.

As the angle of attack increases to α = 5° for x_J/c = 0.08, a separation bubble that extends to $x/c \approx 0.30$ is produced. Streamlines indicate a slight deflection in flow path due to this short separation bubble. Velocity magnitude ahead of the jet location is reduced thereby increasing the local pressure as seen in Fig. 9b. This behavior continues to be exhibited at larger angles. Acceleration of flow at x/c = 0.08 induces greater suction in the region $0.08 \leq x/c \leq 0.2$, however downstream of x/c = 0.20 suction loss is minimal explaining the marginal loss in lift, ΔC_L = -0.05. Upstream of the jet at x_J/c = 0.60, the ejected flow decelerates the flow along the upper surface, mitigating suction up to the separation point caused by the jet. The time-averaged velocity fields show the shear layer initiating ahead of the jet. From Fig. 8, the change in lift coefficient of ΔC_L = -0.18 by the jet at x_J/c = 0.95 is produced by the reduction of suction along the entire upper surface.

Further increase in angle of attack to α = 8° at x_J/c = 0.08, causes the separation bubble to burst leaving a recirculation region, as can be seen in Fig. 8. The local velocity magnitude upstream of the jet is reduced, which is expected to produce a pressure change at the leading edge, and therefore reduce lift, as presented in Fig. 9c. The consequent effect is a lift change of ΔC_L = -0.11. It would ostensibly appear from Fig. 8, that positioning the upstream blowing jet at x_J/c = 0.08 would create a large separated region and would therefore induce a greater loss in lift than blowing case at x_J/c = 0.95. However, Fig. 9c indicates the jet at x_J/c = 0.08 induces a suction loss ahead of the jet, but retains the pressure for the baseline case behind the jet. In contrast, the jet at x_J/c = 0.95 induces a change in lift of ΔC_L = -0.18, by alleviating suction all along the upper surface. Furthermore, at around $x/c \approx 0.65$, boundary layer appears to separate, exhibiting similar performance to when at α = 5°.

From Fig. 8, at α = 13°, for x_J/c = 0.08, the shear layer is deflected upwards at a greater angle which produces a larger wake region. Velocity magnitude ahead of the jet is severely mitigated, as the upper surface pressure reduces significantly in negative pressure as well as indicating flow has separated beyond the jet. In addition, the lower surface experiences suction, thereby explaining the reduction in lift of ΔC_L = -0.33. It follows that, positioning the jet closer to the leading edge has a greater effect on lower surface. Jet at x_J/c = 0.60 and x_J/c = 0.95 produces analogous flow fields, which indicate the jet possesses enough momentum to permeate upstream, up to the point of separation, before impinging with the freestream flow. The interaction between the two opposing flows deflects the shear layer at a greater angle, to evoke a larger recirculation region compared to the baseline case.

D. Effect of Varying Momentum Coefficient

Presented in Fig. 10 are time-averaged velocity fields of baseline cases and upstream blowing with three different momentum coefficients at x_J/c = 0.60. The jet at α = 0° is capable of producing a change in the flow field when tested with the smallest momentum coefficient, C_μ = 0.8%. Acceleration of the flow above the jet is seen to intensify as the momentum coefficient is increased. Furthermore, the high velocity magnitude region close to the leading edge, is seen to diminish with momentum coefficient. However, flow in far field accelerates, with a larger region being influenced with increased momentum coefficient. The subsequent result on the lift curve is minimal, with the C_μ = 0.8% & 4.0% jets producing a change of ΔC_L = -0.02 and ΔC_L = -0.07, respectively.

Increasing the angle of attack to α = 5° and momentum coefficient continues to reduce velocity magnitude near the leading edge region. The shear layer separates downstream of the jet when tested at C_μ = 0.8% & 2.4%, although a momentum coefficient of C_μ = 4.0% initiates the separation upstream of the jet, subsequently augmenting the separated region. Upstream of the accelerated flow caused by the jet, a confined region of significantly reduced velocity magnitude is observed. The reducing effect becomes stronger with momentum coefficient.

Similar behavior to the cases of α = 5° can be observed for α = 8°. All three momentum coefficients are strong enough to induce a separated shear layer on the upper surface. Ostensibly, $C_\mu \geq$ 2.4% is able to provoke separation upstream of the jet. Fig. 11 presents the respective coefficient of pressure plots for upstream blowing at α = 8°. It is evident that the positive pressure gradient becomes more adverse with increasing momentum coefficient. For all cases, suction is reduced upstream of the jet, although aft of the jet, pressure measurements reveal jets of C_μ = 2.4% & 4.0% produce similar suction forces. A lift coefficient reduction of 12.2% is created with a momentum coefficient of C_μ = 2.4%, however this can be augmented to 16.5% with momentum coefficient of C_μ = 4.0%.

The baseline case for α = 13° shown in Fig. 10, ostensibly exhibits a strong separated region. However, this separated region is enlarged once momentum in the opposing direction is introduced, as flow is deflected away from the surface of the airfoil. Velocity magnitude in the near field of the jet is seen to augment with momentum coefficient, suggesting momentum is being transferred within the separated shear layer. It is this behavior that creates the largest change in lift coefficient, as lift is reduced by 26.4% with momentum coefficient of C_μ = 4.0%.

IV. Conclusions

Force, pressure and two-dimensional PIV measurements were performed for two jet configurations on the suction surface of a NACA 0012 wing; normal blowing and upstream blowing. A comparison between blowing directions, for the maximum volumetric flow rate, indicated that upstream blowing is more efficient than normal blowing for the same work; normal blowing effectively reduced lift at x_J/c = 0.95. Upstream blowing amplified this reduction in lift from ΔC_L = -0.15 to ΔC_L = -0.21. The PIV measurements indicate that upstream blowing causes the shear layer to detach ahead of the jet location and consequently modify the aerodynamic camber of the airfoil. This is exhibited at x_J/c = 0.60 where the jet momentum impinges with the opposing freestream flow, evoking flow to deflect away from the airfoil surface. The induced camber change causes flow above the shear layer to accelerate. Pressure measurements indicated that the upstream blowing jet, at all locations, was capable of mitigating suction ahead of the jet. In addition, PIV images confirmed that reduced suction was established through means of alleviating velocity magnitude near the airfoil surface. In addition, it was observed that trailing edge locations are preferable at low angles of attack giving a peak reduction of ΔC_L = -0.22; leading edge locations are preferable at high angles of attack giving a peak reduction of ΔC_L = -0.33.

Acknowledgments

The authors would like to acknowledge the support from an EPSRC studentship, and Airbus UK.

References

[1]Amitay, M., Smith, D. R., Kibens, V., Parekh, D. E., and Glezer, A., "Aerodynamic Flow Control over an Unconventional Airfoil using Synthetic Jet Actuators," *AIAA Journal*, Vol. 39, No. 3, 2001, pp. 361-370.

[2]Tuck, A., and Soria, J., "Separation Control on a NACA 0015 Airfoil using a 2D Micro ZNMF Jet", *Aircraft Engineering and Aerospace Technology*, Vol. 80, No. 2, 2008, pp. 175-180.

[3]Seifert, A., Darabi, A., and Wygnanski, I., "Delay of Airfoil Stall by Periodic Excitation", *Journal of Aircraft*, Vol. 33, No. 4, 1996, pp. 691-698.

[4]Seifert, A., Bachar, A., Koss, D., Shepshelovich, M., and Wygnanski, I., "Oscillatory Blowing: A Tool to Delay Boundary-Layer Separation," *AIAA Journal*, Vol. 31, No. 11, 1993, pp. 2052-2060.

[5]Dimmock, N. A., "An Experimental Introduction to the Jet Flap," Aeronautical Research Council Technical Report C.P. No. 344, 1957.

[6]Goodarzi, M., Rahimi, M., and Fereidouni, R., "Investigation of Active Flow Control over NACA 0015 Airfoil via Blowing," *Internation Journal of Aerospace Sciences*, Vol. 1, No. 4, 2012, pp. 57-63.

[7]Korbacher, G. K., and Sridhar, K., "A Review of the Jet Flap," *UTIA Review: Institute of Aerophysics*, Vol. 14, No. 14, May 1960, pp. 16.

[8]Boeije, C. S., de Vries, H., Cleine, I., van Emden, E., Zwart, G. G. M., Stobbe, H., Hirschberg, A., and Hoeijmakers, H. W. M., "Fluidic Load Control for Wind Turbine Blades," 47th *AIAA Aerospace Sciences Meeting Including The New Horizons Forum and Aerospace Exposition*, 2008, pp. 1-8.

[9]Spence, D. A., "The Lift Coefficient of a Thin, Jet-Flapped Wing," *Proceedings of the Royal Society of London. Series A, Mathematical and Physical Sciences*, Vol. 238, No, 1212, Dec. 1956, pp. 46-68.
[10]Dimmock, N. A., "Some Further Jet Flap Experiments," Aeronautical Research Council Technical Report C.P. No. 345, 1957.
[11]Traub, L. W., and Agarwal, G., "Aerodynamic Characteristics of a Gurney/Jet Flap at Low Reynolds Numbers," *Journal of Aircraft*, Vol. 45, No. 2, 2008, pp. 424-429.
[12]Traub, L. W., Miller, A. C., and Rediniotis, O., "Comparisons of a Gurney and Jet Flap for Hingeless Control," *Journal of Aircraft*, Vol. 41, No. 2, 2004, pp. 420-423.
[13]Greenblatt, D., and Wygnanski, I., "Effect of Leading-Edge Curvature on Airfoil Separation Control," *Journal of Aircraft*, Vol. 40, No. 3, 2003, pp. 473-481.
[14]Barlow, J. B., Rae, W. H., Jr., and Pope, A., *Low-Speed Wind Tunnel Testing*, 3rd ed., John Wiley & Sons, Inc., New York, 1999, pp. 309.
[15]Moffat, R. J., "Using Uncertainty Analysis in the Planning of an Experiment," *Journal of Fluids Engineering – Transactions of the ASME*, Vol. 107, No. 2, 1985, pp. 173-178
[16]Critzos, C. C., Heyson, H. H., and Boswinkle, R. W., Jr., "Aerodynamic Characteristics of NACA 0012 Airfoil Section at Angles of Attack from 0° to 180°," *NACA Technical Note 3361*, Jan. 1955.
[17]Sheldahl, R. E., and Kilmas, P. C., "Aerodynamic Characteristics of Seven Symmetrical Airfoil Sections Through 180-Degree Angle of Attack for use in Aerodynamic Analysis of Vertical Axis Wind Turbines," Sandia National Laboratories SAND80-2114, Mar. 1981.
[18]Jacobs. E. N., and Sherman, A., "Airfoil Section Characteristics as Affected by Variations of the Reynolds Number," NACA Report 586, 1937, pp. 227-267.
[19]Blaylock, M., Chow, R., Cooperman, A., and van Dam, C. P., "Comparison of Pneumatic Jets and Tabs for Active Aerodynamic Load Control," *Wind Energy Journal*, Vol. 17, No. 9, 2014, pp. 1365-1384.
[20]Cooperman, A. M., "Wind Tunnel Testing of Microtabs and Microjets for Active Load Control of Wind Turbine Blades," Ph.D. Dissertation, Mechanical and Aeronautical Engineering Dept., University of California, Davis, 2005.
[21]Lockwood, V. E., and Vogler, R. D., "Exploratory Wind-Tunnel Investigation at High Subsonic and Transonic Speeds of Jet Flaps on Unswept Rectangular Wings," *NACA Technical Note 4353*, Aug. 1958.

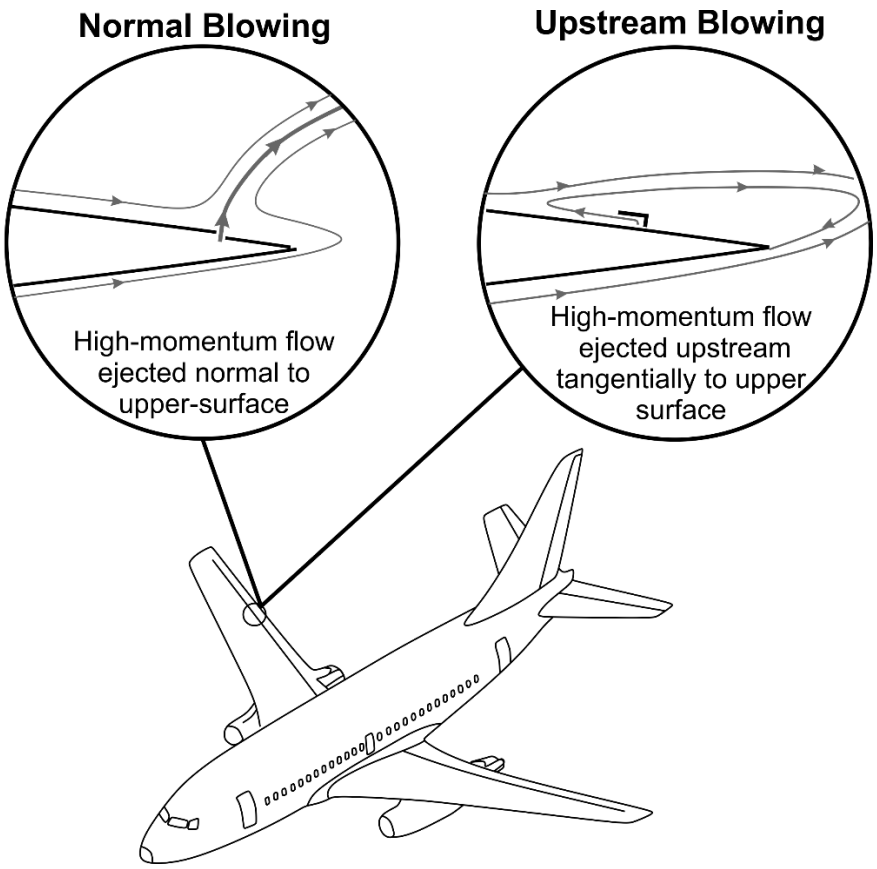

Figure 1. Load control concepts.

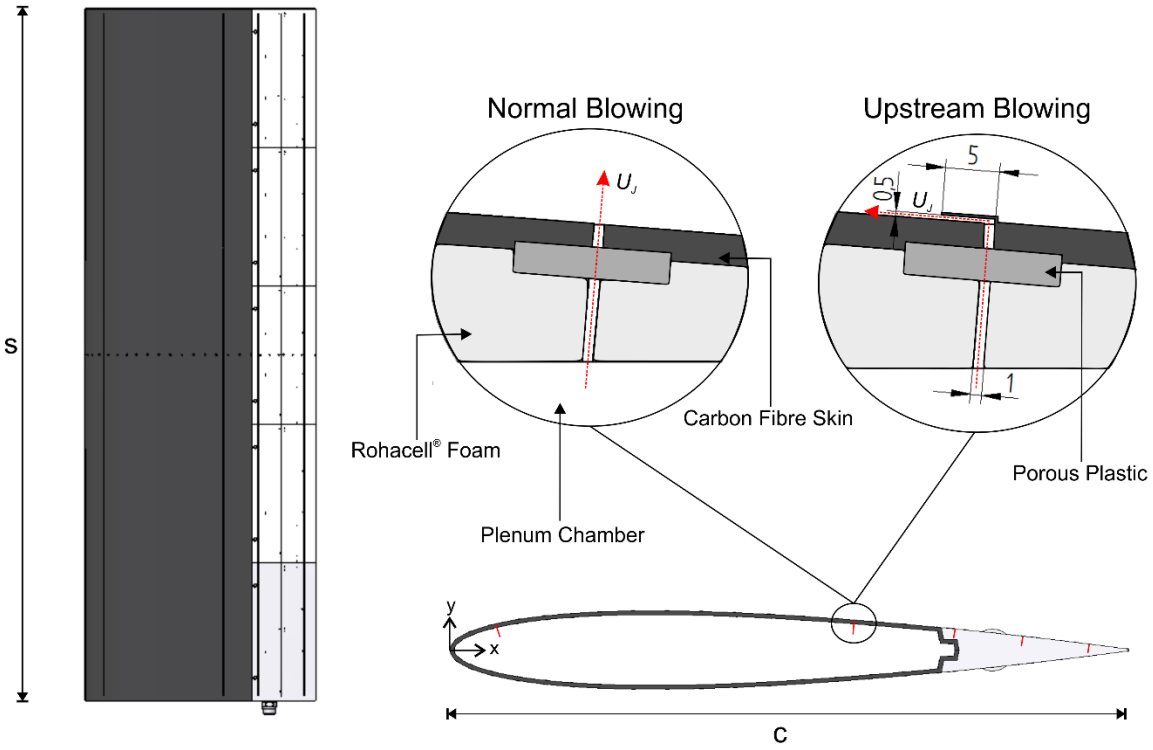

a)

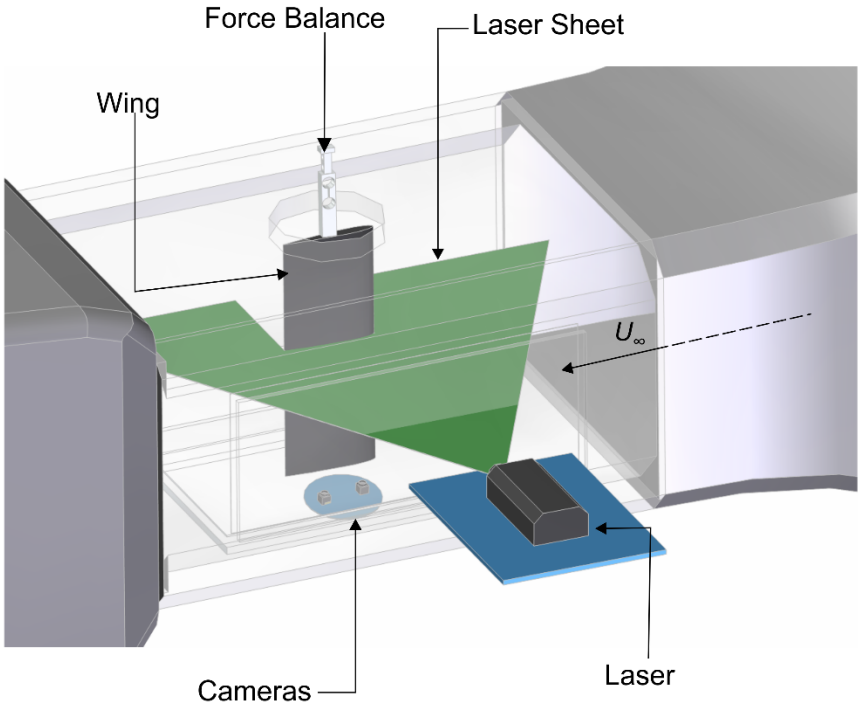

b)

Figure 2. a) Wing setup and chordwise locations of jets, dimensions in millimeters; b) Experimental setup.

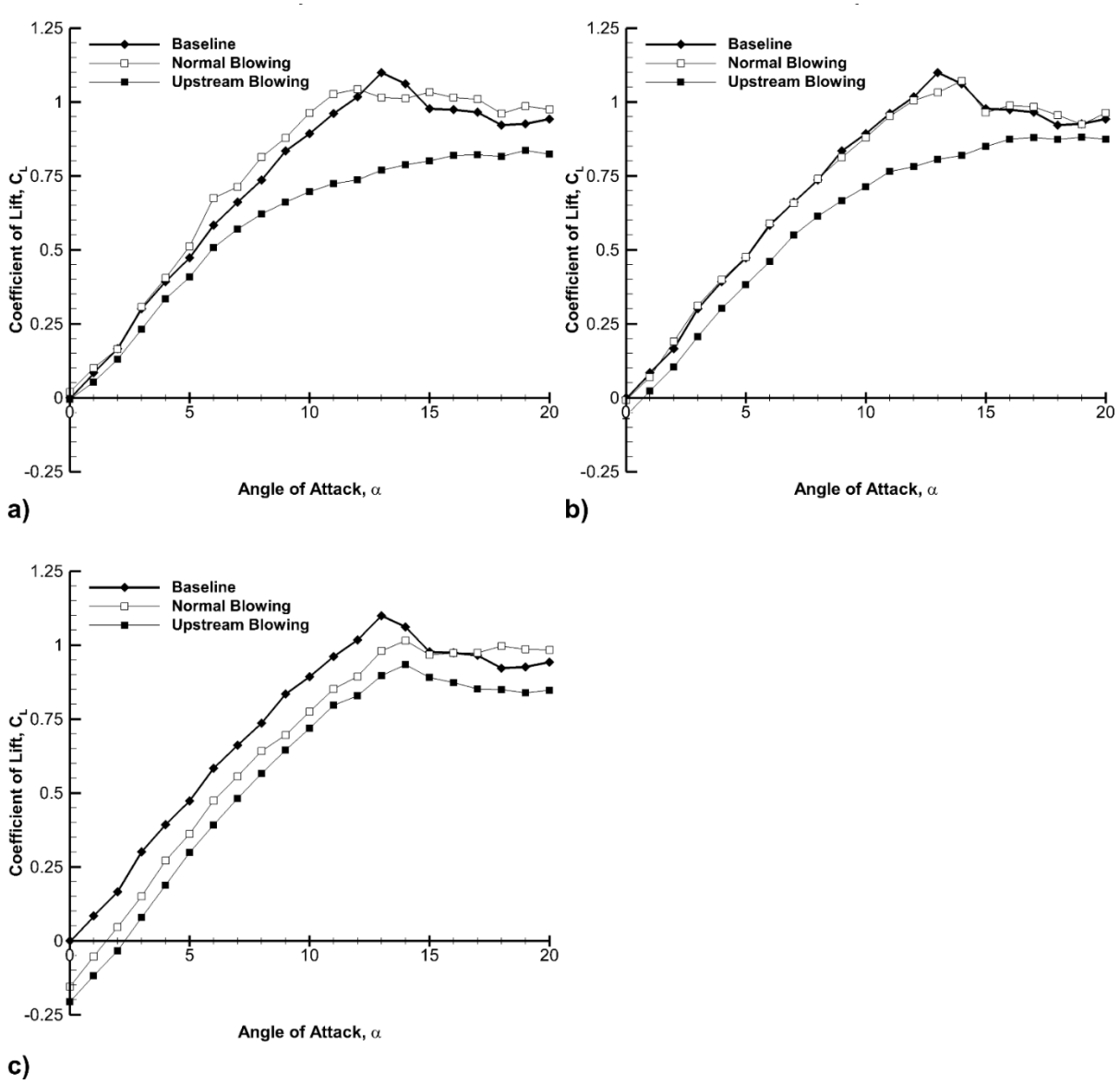

Figure 3. Time-averaged lift coefficient comparing normal blowing (C_μ=2.0%) to upstream blowing (C_μ=4.0%) C_Q = 0.44% for: a) x_J/c = 0.08; b) x_J/c = 0.60; c) x_J/c = 0.95.

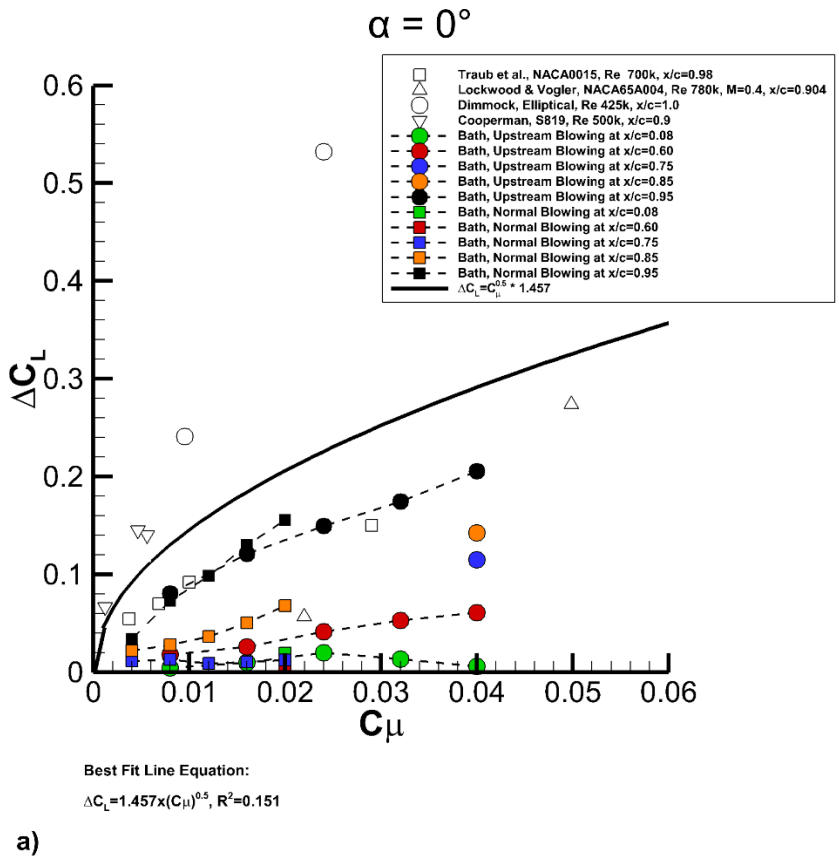

a)

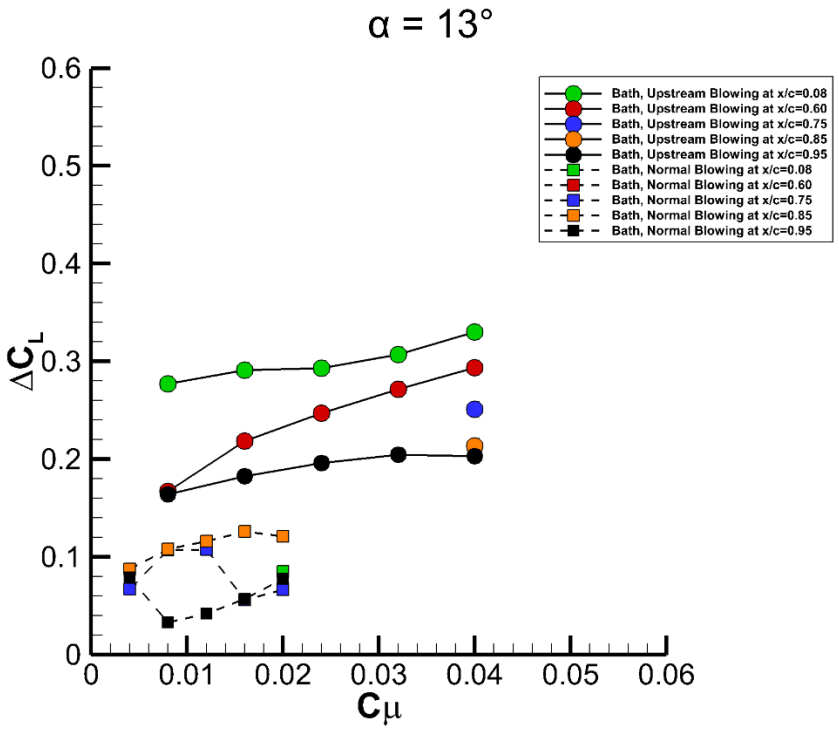

b)

Figure 4. a) Experimental validation with data from the literature for α = 0° and b) α = 13°.

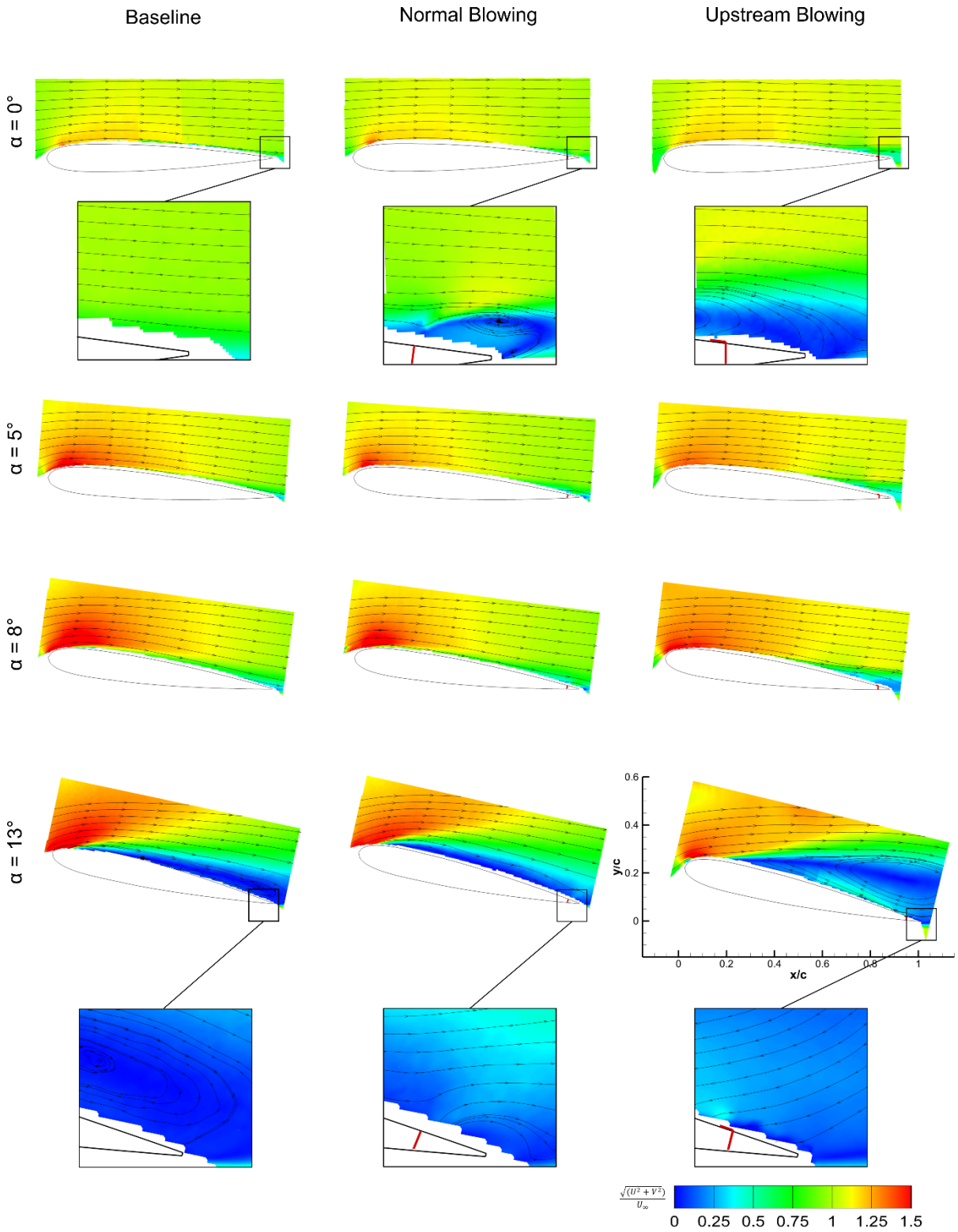

Figure 5. Time-averaged velocity fields comparing normal blowing (C_μ=2.0%) to upstream blowing (C_μ=4.0%) for x_J/c = 0.95, C_Q=0.44% and α = 0°, 5°, 8° & 13°.

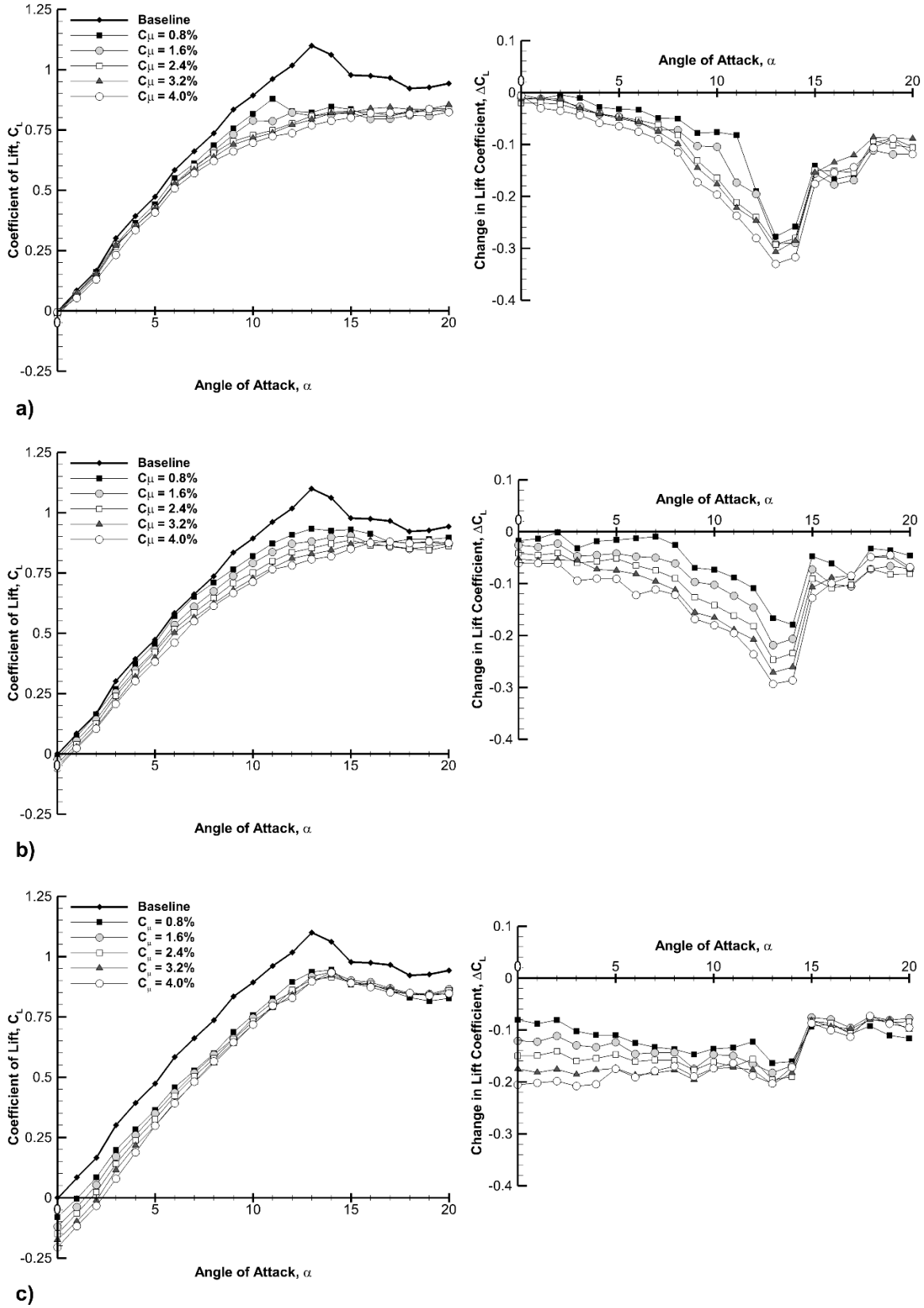

Figure 6. Time-averaged lift coefficient, for upstream blowing, showing the effect varying momentum coefficient a) at x_J/c = 0.08; b) at x_J/c = 0.60; c) at x_J/c = 0.95.

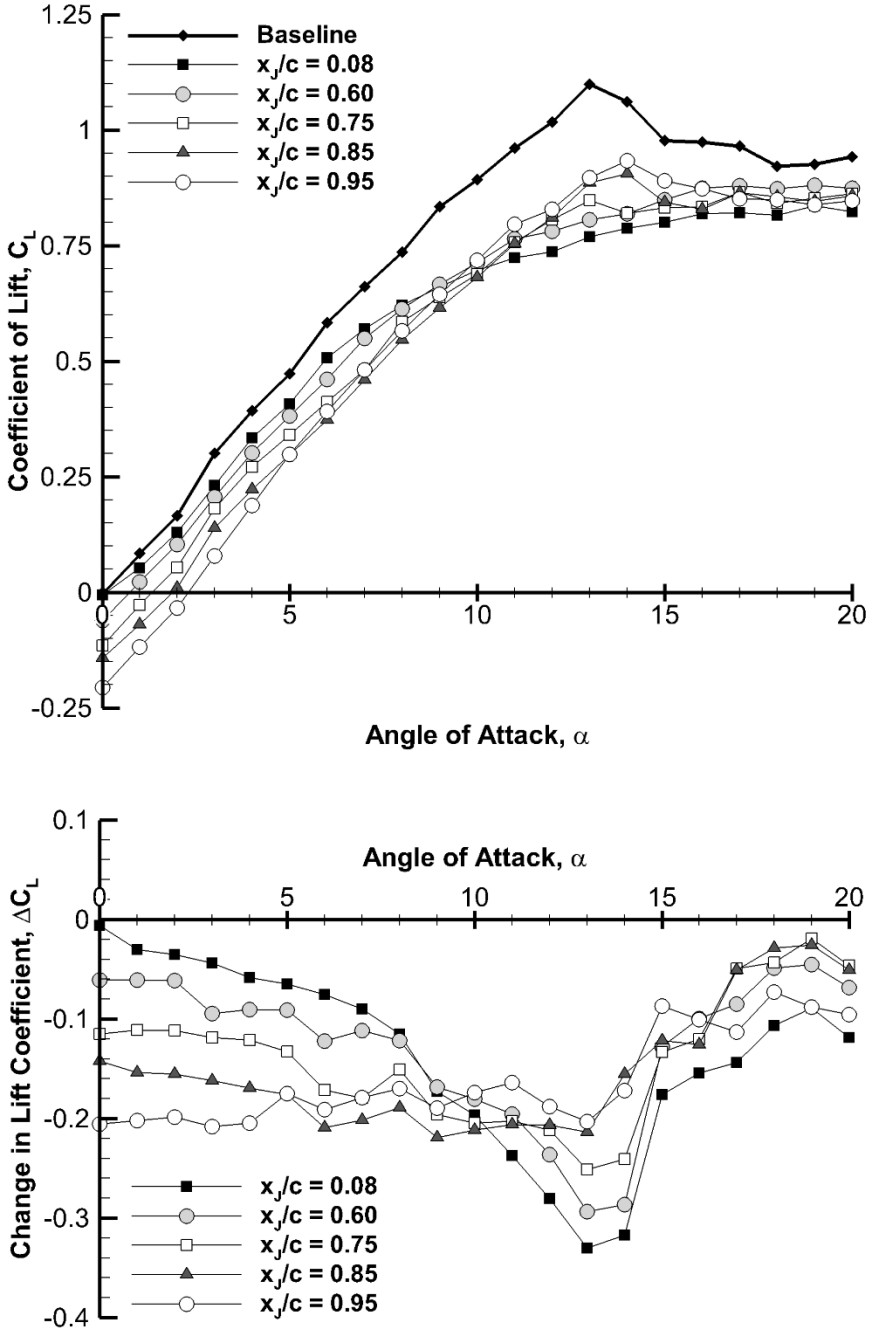

Figure 7. Effect of varying chordwise location for C_μ = 4.0%.

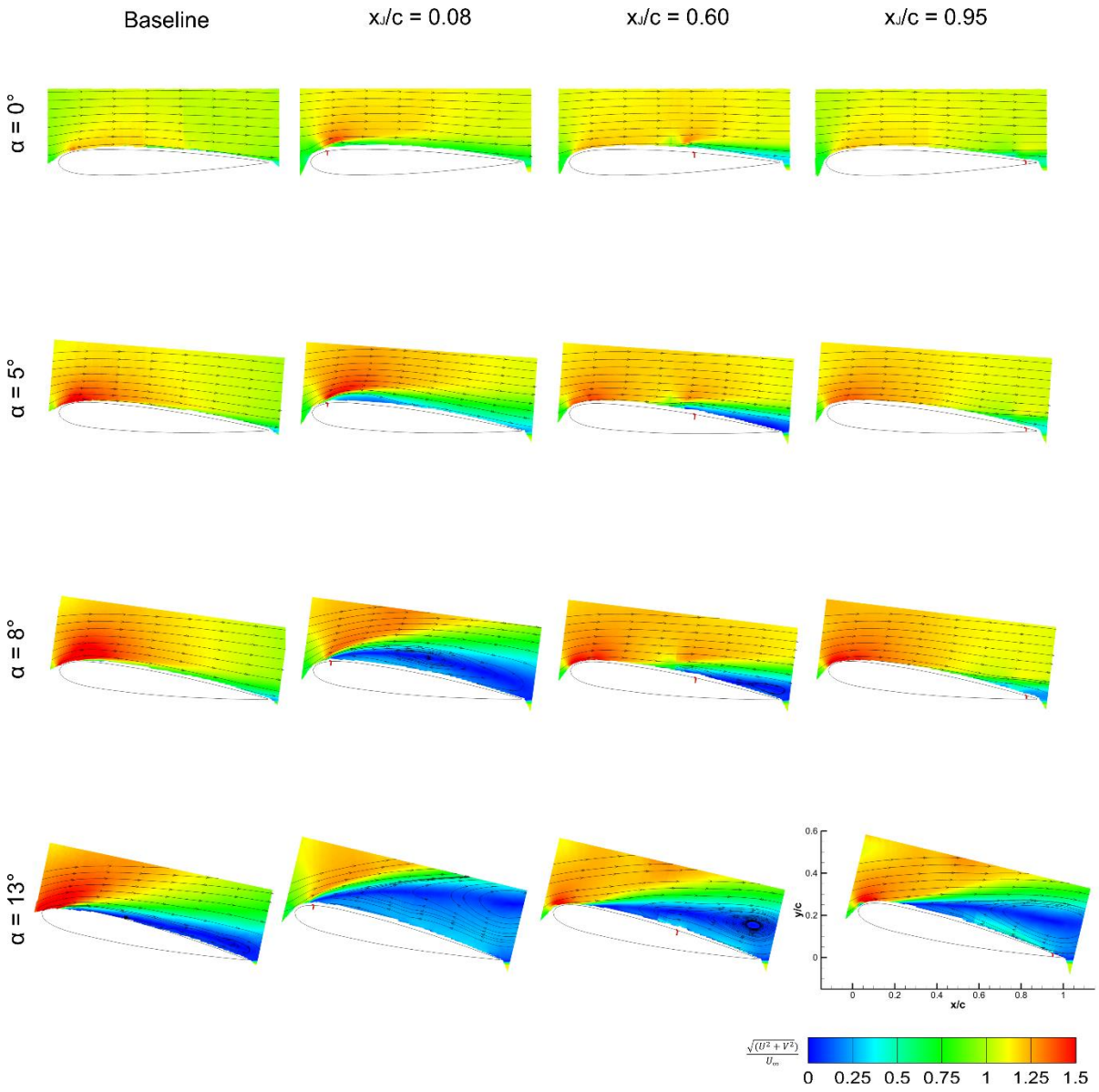

Figure 8. Time-averaged velocity fields for upstream blowing for x_J/c = 0.08, 0.60 & 0.95, C_μ= 4.0% and α = 0°, 5°, 8° & 13°.

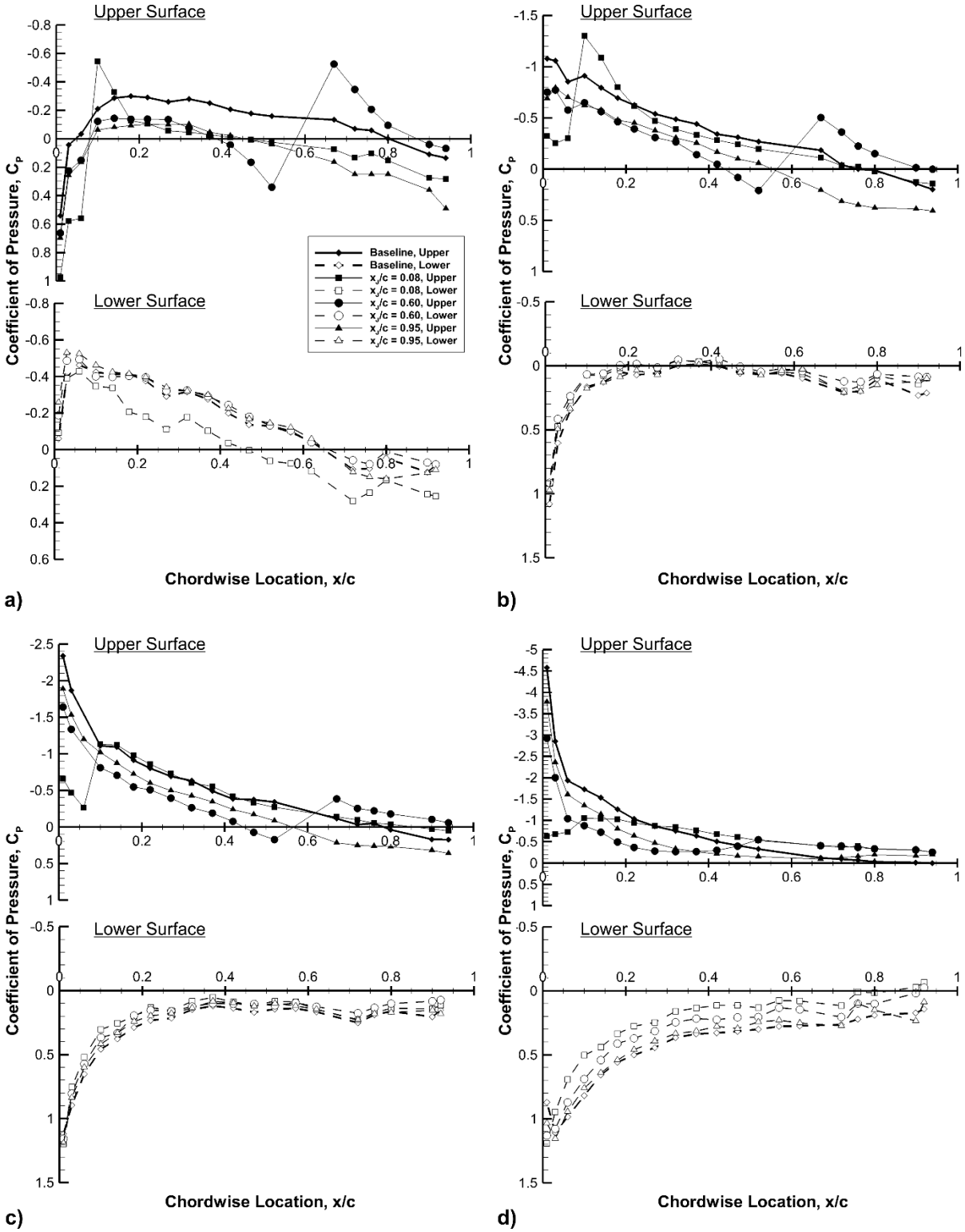

Figure 9. Coefficient of pressure for upstream blowing for x_J/c = 0.08, 0.60 & 0.95, C_μ = 4.0% at: a) α = 0°; b) α = 5°; c) α = 8°; d) α = 13°.

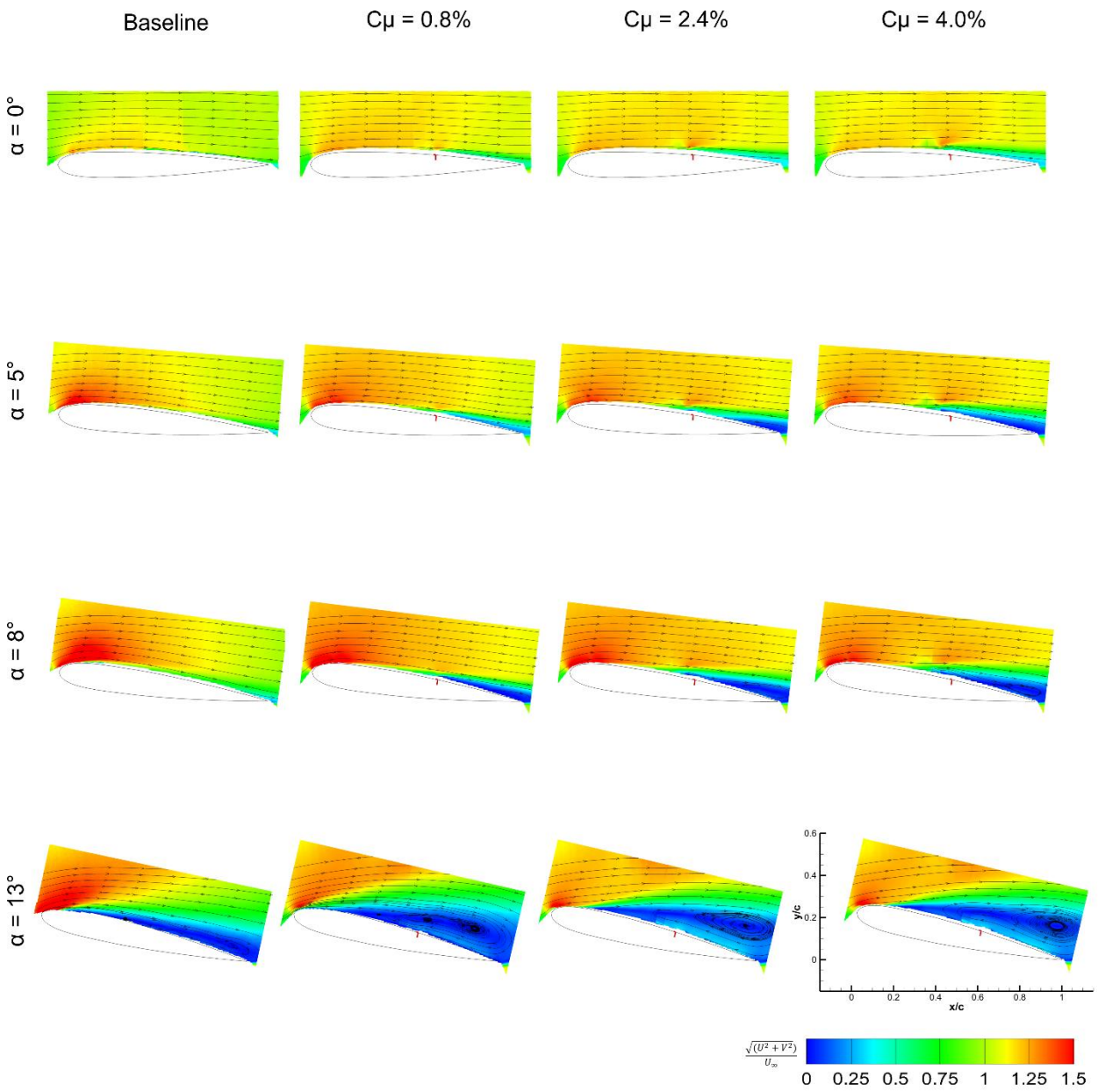

Figure 10. Time-averaged velocity fields for upstream blowing for x_J/c = 0.60, C_μ= 0.8%, 2.4% & 4.0% and α = 0°, 5°, 8° & 13°.

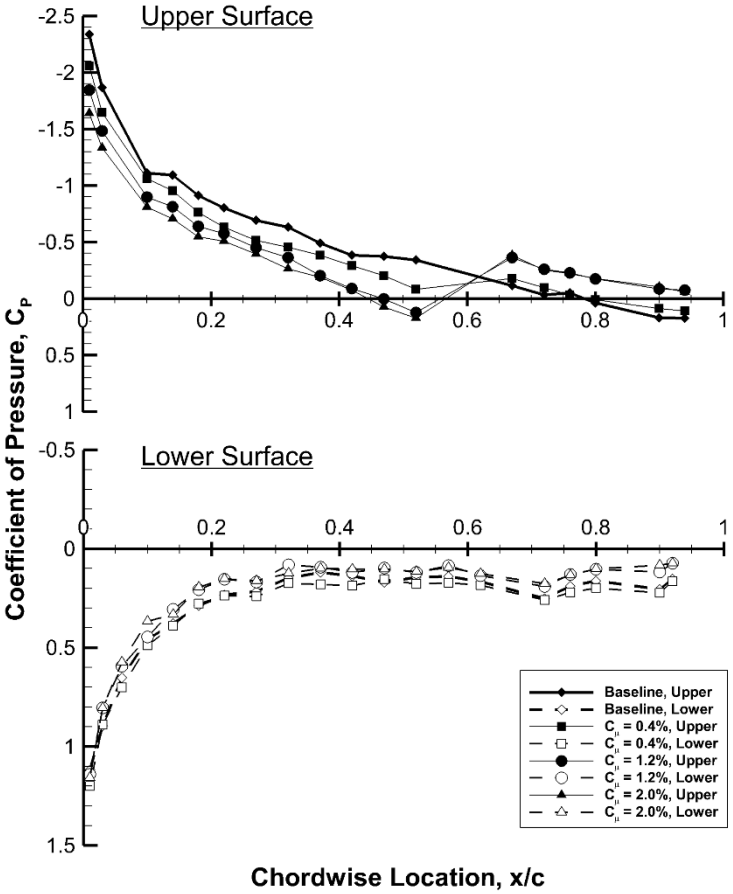

Figure 11. Coefficient of pressure for x_J/c = 0.60, α = 8° for C_μ = 0.8%, 2.4% & 4.0%